Artificial Intelligence-Assisted Optimization and Multiphase Analysis of Polygon PEM Fuel Cells

Ali Jabbary (st_a.jabbary@urmia.ac.ir)
Urmia University https://orcid.org/0000-0003-0573-6909
Nader Pourmahmoud
Urmia University https://orcid.org/0000-0002-9974-6149
Mir Ali Asghar Abdollahi
Urmia University https://orcid.org/0000-0001-8233-6074

Research Article

Keywords: PEM fuel cell, Optimization, CFD, Modeling, Neural network, Performance

Posted Date: April 15th, 2022

DOI: https://doi.org/10.21203/rs.3.rs-1541910/v1

Artificial Intelligence-Assisted Optimization and Multiphase Analysis of Polygon PEM Fuel Cells

Ali Jabbary[a,*], Nader Pourmahmoud[a], Mir Ali Asghar Abdollahi[a]

[a]*Mechanical Engineering Department, Urmia University, Urmia, 5756151818, Iran*

Abstract

This article presents new PEM fuel cell models with hexagonal and pentagonal designs. After observing cell performance improvement in these models, we optimized them. Inlet pressure and temperature were used as input parameters, and consumption and output power were the target parameters of the multi-objective optimization algorithm. Then we used artificial intelligence techniques, including deep neural networks and polynomial regression, to model the data. Next, we employed the RSM (Response Surface Method) method to derive the target functions. Furthermore, we applied the NSGA-II multi-objective genetic algorithm to optimize the targets. Compared to the base model (Cubic), the optimized Pentagonal and Hexagonal models averagely increase the output current density by 21.819% and 39.931%, respectively.

Keywords: PEM fuel cell, Optimization, CFD, Modeling, Neural network, Performance

*Corresponding Author

Email address: st_a.jabbary@urmia.ac.ir (Ali Jabbary)

1. Introduction

Conventional fuel sources cannot fulfill our energy demands today, and their usage pollutes the environment significantly [1]. Renewable energy sources have gained reputations due to sustainability and fewer environmental side-effects [2]. Polymer Electrolyte Membrane Fuel Cells (PEMFCs) have been studied and used by many researchers due to their ability to generate electrical energy from chemical energy and oxidants [3]. PEM fuel cell is the most commonly utilized type of cell because of its quick starting time [4] and convenience in transportation [5], and minor stationary energy requirements [6]. Furthermore, the ever-increasing use of PEM fuel cells needs more research to make it more promising [7].

The challenges that the PEM fuel cell faces are water and thermal management [8, 9, 10, 11, 12, 13, 14, 15], performance optimization [16, 17, 18, 19], design and modeling [18, 20, 21, 22], and cell humidification [23, 24, 25, 26, 27, 28]. One of the critical topics that we can apply to achieve proper performance for the fuel cell is geometric design configuration [29].

Bipolar plates (BP), gas channels, gas diffusion layers (GDL), catalyst layers (CL), and the polymer electrolyte membrane are the five essential components of a PEM fuel cell [3]. The membrane electrode assembly (MEA) is placed between the current collectors. MEA consists of five parts, including a polymer electrolyte membrane, CL, and GDL at each end [16].

The cell's geometric design and flow field play an essential role in fundamental parameters such as how the species are diffused, velocity, temperature and pressure distributions, liquid water content, and current density production [30]. Considerable study has been conducted on the cell structure to

enhance its performance [31]. We can improve mass transfer, temperature diffusion, electrochemical performance and reduce pressure drop by developing an appropriate flow field in the cell [32, 33].

Dong et al. investigated the energy performance of a PEM fuel cell by using discontinuous S-shaped and crescent ribs into flow channels [34]. Asadzade et al. simulated a new bipolar plate based on a lung-inspired flow field for PEM fuel cells to gain higher current densities [35]. Seyhan et al. used artificial neural networks to forecast the cell performance with wavy serpentine channels [36].

Afshari et al. analyzed a zigzag flow channel design for cooling PEM fuel cell plates, and their design provided better temperature control in the cell [37]. Jabbary et al. performed a three-dimensional numerical study on a PEM fuel cell with a rhombus design. The results of this study indicate that the use of this design significantly increases the power and current density [38]. They conducted another study using a new cylindrical configuration on cell performance and water flooding [39]. This design reduces the amount of liquid water in MEA levels and prevents water-flooding.

A great way to increase the performance and output power is geometric or parametric optimization [40]. Optimizing the fuel cell's main parameters before the final operation is one of the most effective ways to reduce production and maintenance costs [41]. Researchers used numerous methods for mathematical optimization in the fuel cell field. Bio-inspired methods like particle swarm [42], whale [43], genetic algorithm [18], Gray Wolf [44], seagull [45], and fish swarm [46] methods are among these.

Cao et al. experimentally analyzed PEM fuel cells using a new, improved

seagull optimization algorithm [47]. In addition, Miao et al. introduced a new optimization method called the Hybrid Gray Wolf Optimizer to obtain the optimal parameters of the PEM fuel cell [48]. Song et al. [49] examined one- and two-parameter numeric optimization analysis of the catalyst layer of the PEM fuel cell to maximize the current density of the catalyst layer with a given electrode potential.

The advantages of using genetic algorithm are [50, 51]:

- Implementation of this theory is simple.
- It searches the population points, not a single point.
- It employs payout data rather than derivatives.
- It provides multi-target optimization.
- It does not utilize deterministic rules but employs probabilistic transitional rules.

We can broadly integrate artificial intelligence (AI) as a fascinating modern technology with most research areas to solve challenges. As a result, this methodology has proved a high potential for advanced improvement in technological growth [52]. AI assists in the enhancement of performance and the development of new enterprise models [53]. Furthermore, we can use embedded AI solutions to optimize manufacturing processes and intelligent functions to extend the machines and services [54]. As a result, artificial intelligence (AI) will be a critical component in the future competitiveness of mechanical engineering products and processes.

This study introduces new models of pentagonal and hexagonal fuel cells. We used artificial intelligence-based optimization methods to investigate the effects of critical parameters on current density and output/consumed powers in multiphase mode. We also perform analyzes based on pressure, temperature, velocity, and water content of the MEA on the cell to achieve the performance of these models. This study aims to achieve maximum output power while maintaining minimum consumed power.

2. Methodology

2.1. Physical Model

We employed the fuel cell model based on CFD methods, allowing the physical and electrochemical phenomena in the cell to be numerically solved. The base design of the fuel cell (Cubic) and the polygon models used in this research are shown in Figure 1, which shows the cell's main components.

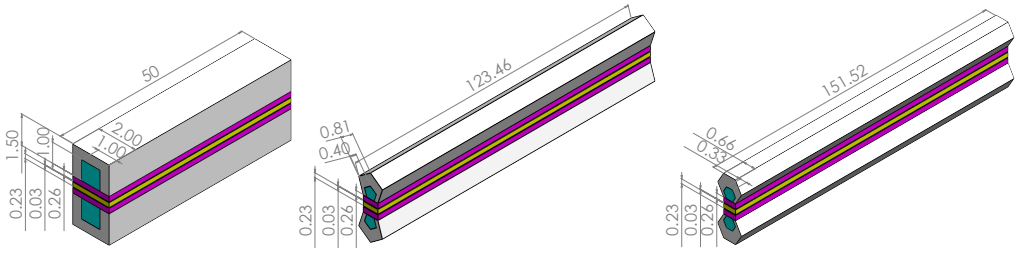

(a) Cubical model (b) Pentagonal model (c) Hexagonal model

Figure 1: PEM fuel cell models

The sizes and geometric specifications are displayed on this figure and are described in Table 1.

Table 1: Geometric specifications of the presented models

Parameter	**Unit**	**Cubical**	**Pentagonal**	**Hexagonal**
Channel side	mm	1	0.4	0.33
Channel length	mm	50	123.46	151.52
BP side	mm	1.5—2	0.81	0.66
GDL thickness	mm	0.26	0.26	0.26
CL thickness	mm	0.03	0.03	0.03
Membrane thickness	mm	0.23	0.23	0.23
MEA wet area	mm^2	100	100.002	100.002
Inlet/Outlet area	mm^2	1	0.28	0.28

2.2. Model Assumptions

A *comprehensive fuel cell* is a highly complex device that includes fluid dynamics, mass transport phenomena, and electrochemical processes. To respond to a three-dimensional model problem, we must assume the following reasonable simplification assumptions [55]:

- Channel flows are assumed to be laminar, incompressible, and steady;
- PEMFC operates in non-isothermal, multiphase, and steady-state situations;
- GDL and CL are isotropic and homogenous;
- The MEA (membrane electrode assembly) is homogenous porous media with uniform porosity;

- The membrane is entirely humidified, ensuring consistent ionic conductivity.

2.3. Governing Equations

We should investigate numerous connected phenomena in various cell components to analyze performance, such as reactant flow, species transfer, reactant consumption, water production, temperature, pressure diffusions, and electric power generation. We applied a three-dimensional steady-state model to investigate the various phenomena.

2.3.1. Continuity equation

The conservation of mass equation (continuity) in all regions is calculated this way [56];

$$\frac{\partial(\rho u)}{\partial x} + \frac{\partial(\rho v)}{\partial y} + \frac{\partial(\rho w)}{\partial z} = 0 \tag{1}$$

Electrodes are manufactured by carbon cloth, or carbon fiber [57]. Therefore, they are recognized as a porous medium where distributed reactant gases (species). Concerning the porosity of MEA (ϵ), the continuity equation is formulated as follows:

$$\frac{\partial(\rho\epsilon u)}{\partial x} + \frac{\partial(\rho\epsilon v)}{\partial y} + \frac{\partial(\rho\epsilon w)}{\partial z} = S_m \tag{2}$$

u, v, and w are velocity in the x, y, and z axes, individually, ρ is the density of reactant gases. S_m is the mass sink/source term, and it is considered zero since no reaction occurs in the flow channels and GDLs. However, because of the reactivity of reactant species, the sink/source term is not zero in the catalyst layer and can be evaluated using the following equations [58]:

$$S_{H_2} = -\frac{M_{H_2}}{2F} R_a \tag{3}$$

$$S_{O_2} = -\frac{M_{O_2}}{4F} R_c \tag{4}$$

$$S_{H_2O} = -\frac{M_{H_2O}}{2F} R_c \tag{5}$$

F is the Faraday constant ($96,485 \frac{C}{mol}$), and M is the species' molecular weight ($\frac{kg}{mol}$) and R can be calculated by Butler–Volmer equations (18 and 19).

2.3.2. Momentum Equations

The momentum conservation equations are described below:

$$\nabla.(\rho\vec{u}\vec{u}) = -\nabla P + \nabla.(\mu\nabla\vec{u}) + S_{p,i} \tag{6}$$

$S_{p,i}$ is the sink/source term for porous media in the x, y, and z axes. As the pressure decreases in porous media, Darcy's law has been estimated in the model. The source term is determined as [59]:

$$S_{p,i} = -\left(\sum_{j=1}^{3} \frac{1}{\beta_j} \mu u_j\right) \tag{7}$$

β is the permeability of the media.

2.3.3. Energy Conservation

The energy conservation equation can be expressed as follows:

$$\nabla.\left(\vec{v}\left(\rho E+P\right)\right)=\nabla.\left(k_{\text{eff}}\nabla T-\sum_{j=1}h_j\vec{j_j}+\left(\tau_{\text{eff}}.\vec{v}\right)+S_h\right) \tag{8}$$

Total energy, enthalpy, and effective shear tensor are denoted by E, h, and τ_{eff}, respectively. k_{eff} is effective conductivity in porous media, computed as the volume average of solid and fluid conductivity:

$$k_{\text{eff}}=\epsilon k_f+(1-\epsilon)k_s \tag{9}$$

S_h is the sink term in the energy equation and can be calculated as follows:

$$S_h=h_{\text{phase}}+h_{\text{reaction}}+R_{\text{ohm}}I^2 \tag{10}$$

The model removed the h_{phase} term since simulations did not account for phase change. The ohmic term is estimated because there is no heat production operator in bipolar plates. As a result, the energy equation is reduced to the following:

$$\nabla.(k\nabla T)=-R_{ohm}I^2 \tag{11}$$

k is the conductivity of the bipolar plates.

2.3.4. Mass Transfer (Species Transport Equations)

The reactant gases are hydrogen and air, which are ideal gases. The following are the equations for species transport:

$$\nabla.\left(\epsilon\vec{u}C_i\right)=\nabla.\left(D_i^{eff}\nabla C_i\right)+S_i \tag{12}$$

C_i is the species' molar concentration. S_i is the extra volumetric source term of species such as H_2, O_2, and H_2O for CLs zones and are calculated by;

$$S_{\mathrm{H_2}} = -\frac{R_a}{2F} \tag{13}$$

$$S_{\mathrm{O_2}} = -\frac{R_c}{4F} \tag{14}$$

$$S_{\mathrm{H_2O}} = \frac{R_c}{2F} \tag{15}$$

In addition, the gas diffusivity coefficient (D_i^{eff}), which is determined by operation conditions, is provided by;

$$D_i^{\mathrm{eff}} = \epsilon^{0.5}(1-s)^{r_s} D_i^{\mathrm{eff}} \left(\frac{P_0}{P}\right) \left(\frac{T}{T_0}\right)^{\frac{2}{3}} \tag{16}$$

r_s is the saturation exponent of pore blockage, D_i^{ref} is the reference mass diffusivity of the i_{th} species under standard conditions, and s is water saturation (the volume percentage of liquid water) and is derived as follows;

$$s = \frac{V_{\mathrm{liquid}}}{V_{\mathrm{total}}} \tag{17}$$

Here, V is the volume.

2.3.5. Butler–Volmer Equation

The Butler-Volmer equation can define the volumetric transfer currents are given by;

$$R_a = \left(\zeta_a j_a^{\mathrm{ref}}\right)_a \left(\frac{C_{\mathrm{H_2}}}{C_{\mathrm{H_2}}^{\mathrm{ref}}}\right)^{\gamma_a} \left(e^{\frac{\alpha_a F \eta_a}{RT}} - e^{\frac{-\alpha_c F \eta_a}{RT}}\right) \tag{18}$$

$$R_c = \left(\zeta_c j_c^{\mathrm{ref}}\right)_c \left(\frac{C_{\mathrm{O_2}}}{C_{\mathrm{O_2}}^{\mathrm{ref}}}\right)^{\gamma_c} \left(e^{\frac{\alpha_a F \eta_c}{RT}} - e^{\frac{-\alpha_c F \eta_c}{RT}}\right) \tag{19}$$

The values j^{ref}, ζ, and α represent the reference exchange current density, specific active surface area, and transfer coefficient. In addition, c, c_{ref}, and γ represent the concentration of reactant flow, the reference value, and the concentration dependency, respectively.

2.3.6. Charge Conservation Equations

Electrochemical processes take place at the catalyst layers in PEM fuel cells. Surface activation overpotential is the main factor behind these responses [60]. Therefore, the potential difference between the solid and the membrane is referred to as the activation overpotential [61]. As a consequence, two charge equations are required. One equation for electron transport via conductive solid phase and another for proton transport across the membrane:

$$\nabla.\left(\sigma_{sol}\nabla\phi_{sol}\right) + R_{sol} = 0 \tag{20}$$

$$\nabla.\left(\sigma_{mem}\nabla\phi_{mem}\right) + R_{mem} = 0 \tag{21}$$

Current density (A/m3) is used to describe volume sink terminology. Only in the catalytic layers are these expressions set. For the solid phase, they are calculated by:

Anode side:

$$R_{sol} = -R_a \quad (< 0) \tag{22}$$

Cathode side:

$$R_{sol} = -R_c \quad (> 0) \tag{23}$$

For the membrane phase, they can be evaluated by the following equations:

Anode side:

$$R_{mem} = -R_a \quad (> 0) \tag{24}$$

Cathode side:

$$R_{mem} = -R_c \quad (< 0) \tag{25}$$

The following equation is used to determine average current density:

$$i_{ave} = \frac{1}{A}\int_{V_a} R_a dV = \frac{1}{A}\int_{V_c} R_c dV \tag{26}$$

2.3.7. Water Transport via Membrane

Water produced by the cathodic process in PEM fuel cells diffuses to the anode side. It will transport across the membrane via electro-osmosis force and back diffusion [62]. λ is determined as the number of water molecules divided by the number of charged HSO_3 sites. Springer et al. [63] developed a formula for estimating it:

$$\lambda = \begin{cases} 0.043 + 17.81a - 39.85a^2 + 36a^3 & 0 \leq a \leq 1 \\ 14 + 1.4(a-1) & 0 \leq a \leq 3 \end{cases} \tag{27}$$

a denotes the water activity.

2.3.8. Consumption and Production Powers

The consumption and production powers are two important parameters affecting the performance of the PEM fuel cell. In section 3, we will obtain these values and analyze them. We can calculate these parameters by the following equations [38]:

- Production power:

$$P_{pro} = I.V.A_{eff} \tag{28}$$

- Consumption power:

$$P_{cons} = \Delta P.A_{in}.u_{in} \tag{29}$$

Here, A_{eff} is the effective area of the membrane and, A_{in} is the inlet area of the channel.

2.4. Simulation Conditions

Table 2 presents the initial operating conditions that we utilized for numerical simulation. We applied the same initial operating conditions to all models.

Table 2: Operating conditions

Parameter	**Unit**	**Value**
Operating pressure	atm	101325
Operating temperature	K	353.15
Anode relative humidity	–	100%
Cathode relative humidity	–	100%
Anode stoichiometry	–	1.2
Cathode stoichiometry	–	2

The boundary conditions of the models are given in Table 3, and the specifications of the MEA layers are shown in Table 4 according to Hashemi's study [64].

2.5. Numerical Procedure

Figure 2 displays the presented CFD algorithm of PEM fuel cell simulation. We used ANSYS® Fluent 2021 R1 software in our CFD analysis to solve

Table 3: Boundary conditions

Parameter	**Unit**	**Cubical**	**Pentagonal**	**Hexagonal**
Anode mass flow rate	kg/s	1.32597e-07	1.333e-07	1.3193e-07
Cathode mass flow rate	kg/s	1.39212e-06	1.3995e-06	1.38516e-06
H_2 mass fraction at anode inlet	–	0.11345436	0.11345436	0.113454
H_2O mass fraction at anode inlet	–	0.88654564	0.88654564	0.886546
O_2 mass fraction at cathode inlet	–	0.1506207	0.150620732	0.150621
H_2O mass fraction at cathode inlet	–	0.3532008	0.35320078	0.353201
Inlet pressure	atm	1	1	1
Relative inlet humidity	–	100%	100%	100%
Inlet temperature at anode/cathode	K	353.15	353.15	353.15

Table 4: Membrane Electrode Assembly (MEA) properties

Parameter	**Symbol**	**Unit**	**Value**
GDL porosity	ϵ_{GDL}	–	0.5
CL porosity	ϵ_{CL}	–	0.5
Membrane porosity	ϵ_{mem}	–	0.6
Electrical conductivity of electrode	σ_{sol}	S/m	100
Proton conductivity of membrane	σ_{mem}	S/m	17.1223
Thermal conductivity of electrode	k_{eff}	W/mK	1.3
Anode apparent charge transfer coefficient	α_{an}	–	0.5
Cathode apparent charge transfer coefficient	α_{cat}	–	1.0
Anode exchange current density	$R_{\text{an}}^{\text{ref}}$	A/m^2	30.0
Cathode exchange current density	$R_{\text{cat}}^{\text{ref}}$	A/m^2	0.004

the governing equations through the computational domain using the finite volume method. We applied the double-precision technique and the second-

order upwind method to discretize the terms. In addition, we employed the multigrid *F-Cycle* type [65] and the *BCGSTAB* method (Biconjugate Gradient Stabilized Method) with 50 max course cycles to stabilize the solutions and avoid divergence due to the complex nature of the governing equations.

Stopping criteria are requirements that must be met for the algorithm to be stopped. Considering that an iterative approach computes successive approximations to a nonlinear system's solution, a test is required to decide when to terminate the iteration. Stopping criteria would evaluate the distance between the latest iteration and the correct answer. These distances are called residuals. The lower the value of residuals, the closer the numerical analysis results to the existing solutions with fewer errors. When the residuals reach the desired value, the iteration is over, and we will obtain the final results.

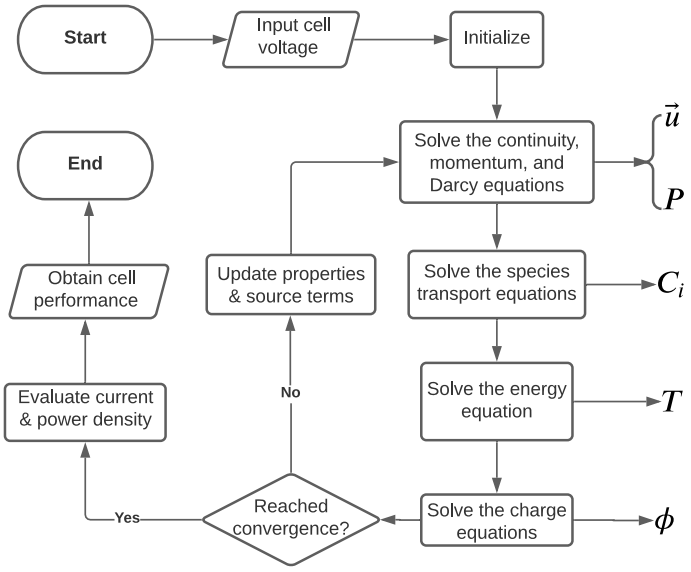

Figure 2: CFD algorithm of PEM fuel cell simulation

2.6. Artificial Intelligence-Assisted Optimization

Mathematical optimization is an effective method for resolving complex problems by utilizing the most efficient resources and data. Optimization is the process of determining the values of decision variables to achieve a problem's goal. One of the most important applications of artificial intelligence is lowering the computing costs of optimization. An optimization model comprises appropriate objectives, variables, and constraints. The most reliable solution is choice variables that maximize or minimize the objective function while remaining within the solution range. The objectives of this study are the produced and consumed powers. We used *Feed-forward deep neural networks* to model the data. *Response Surface Method (RSM)* was applied for function approximation to extract objective functions and use them in the optimization algorithm.

2.6.1. Machine Learning Model

Figure 3 shows the presented deep neural network for modeling the objectives and variables. We created a sequential model for the neural network using Tensorflow [66]. The mentioned neural network has two input neurons (inlet temperature and inlet pressure) and one output neuron (once for produced power and once for consumed power) with two hidden layers, each with ten neurons. We used *relu* activation function for the hidden layers. After modeling the data, we applied two-dimensional polynomial regression to obtain the objective functions.

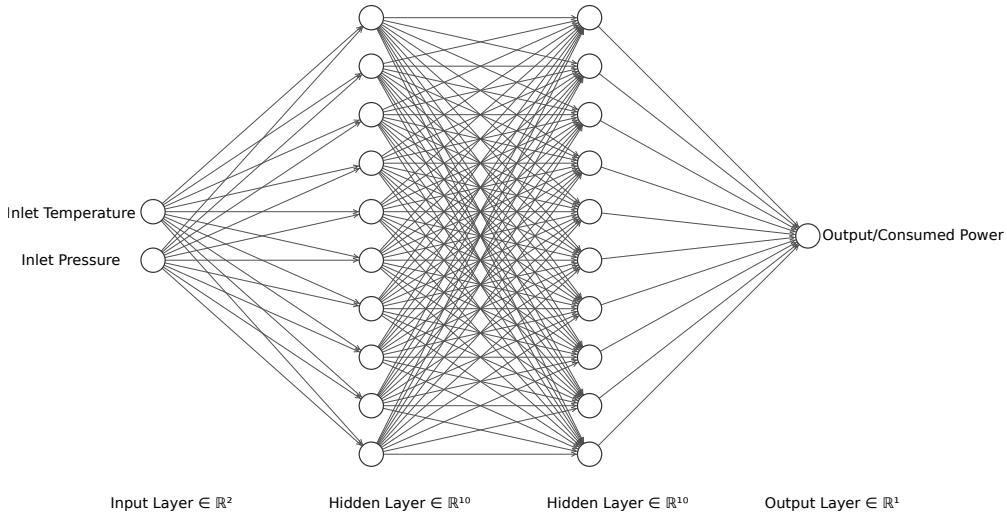

Figure 3: Presented Feed-Forward neural network

2.6.2. Genetic Algorithm

The genetic algorithm is a heuristic optimization strategy that replicates natural evolution by changing a population of individual solutions [67]. Chromosomes represent design points (x). The method selects parents randomly from the existing population and uses them to produce the next generation. Since good parents produce good children, the population gradually approaches an ideal solution over successive generations. The algorithm eliminates the bad points from the generation. GA can achieve the optimal global solution without clinging to a locally optimal solution. Because GA is a probabilistic method, different runs may yield different results. As a result, we require many runs to validate the best solution.

The genetic algorithm consists of five stages:

- **Initial population:** The procedure starts with a group of data identified as a population. Each case is a potential solution to the addressed

problem; Genes are a set of characteristics (variables) that describe a person. Chromosomes comprise a string of genes (solution).

- **Fitness function:** The fitness function defines an individual's fitness level. It assigns each case a fitness score, and the fitness score determines the likelihood of an individual being chosen for regeneration.
- **Selection:** This stage aims to choose the fittest individuals and pass on their genes to the next generation. Two sets of individuals are selected depending on overall fitness levels. Individuals with high fitness scores are more likely to be determined for regeneration.
- **Crossover:** Crossover is the most critical stage. A crossover point is a randomly selected point within the genes for each couple of parents to be matched.
- **Mutation:** The mutation stage is to conserve population variety and to prevent early convergence.

We will terminate the algorithm and obtain the solutions when we reach population convergence.

3. Results and Discussion

This section will present the results and analyze the fundamental parameters of the models and compare them with each other. The grid Independence test and model validation are explained in our previous work [38].

3.1. Optimization

We mathematically optimized the desired parameters of the problem. The input parameters of this research are the inlet pressure and temperature of the cell, and the output parameters are power consumption and production power. Our goal is to maximize output power while maintaining/minimizing power consumption. To do this, we changed the inlet pressure from 1 *atm* to 5 *atm* and at the same time, the inlet temperature from 50°C to 90°C step by step. In each stage, we calculated the consumption and production powers. Figure 4 shows the changes in these powers with different pressures and temperatures in 3d space.

Production power in both models has the highest values at all temperatures and a pressure of 1 atmosphere—the higher the inlet pressure, the lower the production power. Figure 5 shows the two-dimensional contours of these results. As shown, the power consumption in the two models, at all pressures and a temperature of 90°C, has its maximum values. By decreasing the temperature, we can reduce the power consumption of the fuel cell.

To perform multi-objective optimization, we first modeled the data using the neural network mentioned in Figure 3. Then by multi-parameter polynomial regression, we derived the mathematical relationships of the problem objectives. The relationships for power production are as follows:

Pentagonal Model:

$$P_{pro} = 3.266e^{-6}P^2 + 5.816e^{-8}PT - 3.127e^{-5}P - 1.928e^{-8}T^2 + 2.936e^{-6}T - 3.027e^{-5} \quad (30)$$

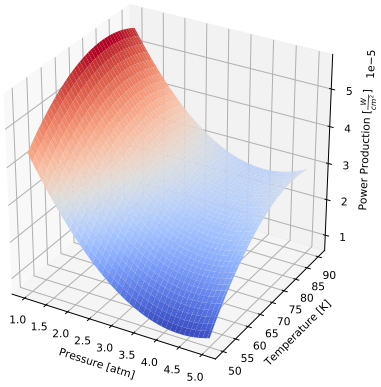

(a) $P_{pro.}$ of Pentagonal Model

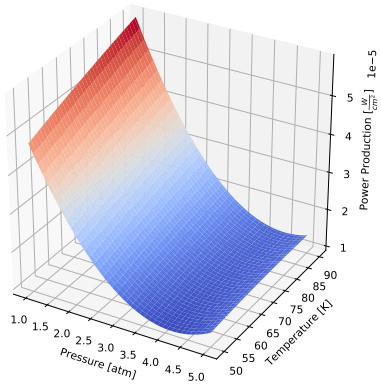

(b) $P_{pro.}$ of Hexagonal Model

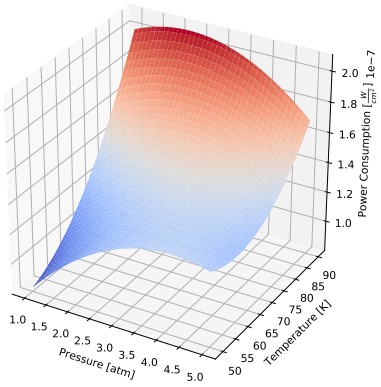

(c) $P_{cons.}$ of Pentagonal Model

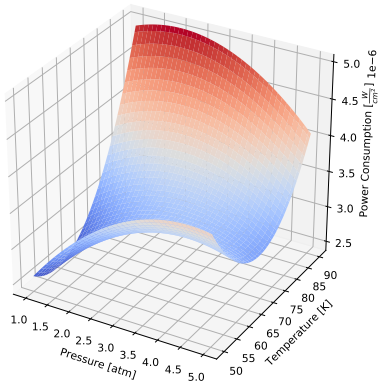

(d) $P_{cons.}$ of Hexagonal Model

Figure 4: Changes of production/consumption power of models

Hexagonal Model:

$$P_{pro} = 3.82e^{-6}P^2 - 6.802e^{-8}PT - 2.82e^{-5}P - 9.945e^{-10}T^2 + 5.052e^{-7}T + 5.251e^{-5} \quad (31)$$

And the relationships for power consumption are as follows:

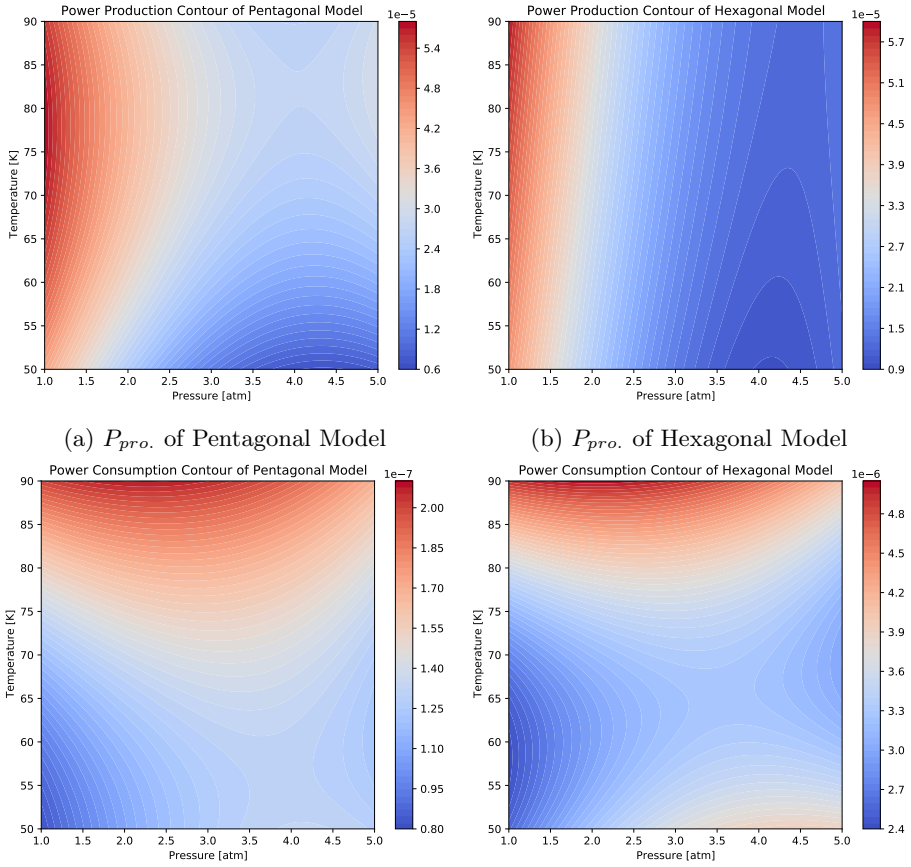

(a) $P_{pro.}$ of Pentagonal Model

(b) $P_{pro.}$ of Hexagonal Model

(c) $P_{cons.}$ of Pentagonal Model

(d) $P_{cons.}$ of Hexagonal Model

Figure 5: Contours of production/consumption power of models

Pentagonal Model:

$$P_{cons} = -5.112e^{-9}P^2 - 4.847e^{-10}PT + 6.669e^{-8}P + 5.415e^{-11}T^2 - 4.154e^{-9}T + 1.172e^{-7} \quad (32)$$

Hexagonal Model:

$$P_{cons} = -1.111e^{-7}P^2 - 1.365e^{-8}PT + 1.68e^{-6}P + 2.4647e^{-9}T^2 - 2.729e^{-7}T + 9.1835e^{-6} \quad (33)$$

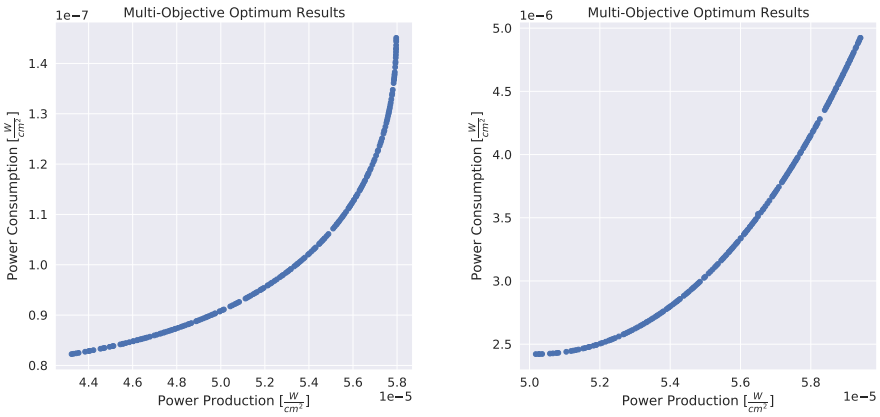

(a) Pentagonal Model (b) Hexagonal Model

Figure 6: Comparison of optimization results

After obtaining the objective functions of the problem, we used the *NSGA-II* multi-objective genetic algorithm to optimize the objectives. We set 200 generations, a population size of 200, and a seed of 1. Figure 6 shows the results of this optimization as the optimal range between the two objective functions. According to this figure, in both models, the higher the production power, the higher the fuel cell's consumption power. To find reasonable values for the input parameters of the problem, we need to examine these results. In both models, the device's power consumption is much less than the production power. This value is 0.198% of the production power on average in the Pentagonal model and 6.21% of the production power on average in the Hexagonal model. Considering this, if the maximum production power is available in both models, the power consumption in the Pentagonal model is only 0.25% of the production power. In comparison, the power consumption in the Hexagonal model is 8.29% of the production power. As a result, if we use the input parameters to achieve maximum output power, power consumption

will still be much lower. In this case, the inlet pressure and temperature in the Pentagonal model will be 1 atm and 77.645 °C, and in the Hexagonal model, 1 atm and 90 °C, respectively.

3.2. Polarization Curves and Current Density

Fig 7 shows the polarization curves of the presented models. The presented models produced more current and power density than the Cubic model. The performance of the optimized models in this field is more than the standard models due to optimized parameters. To be able to compare these values accurately, Table 5 and Figure 8 indicate the percentage increase in the current density of the proposed models.

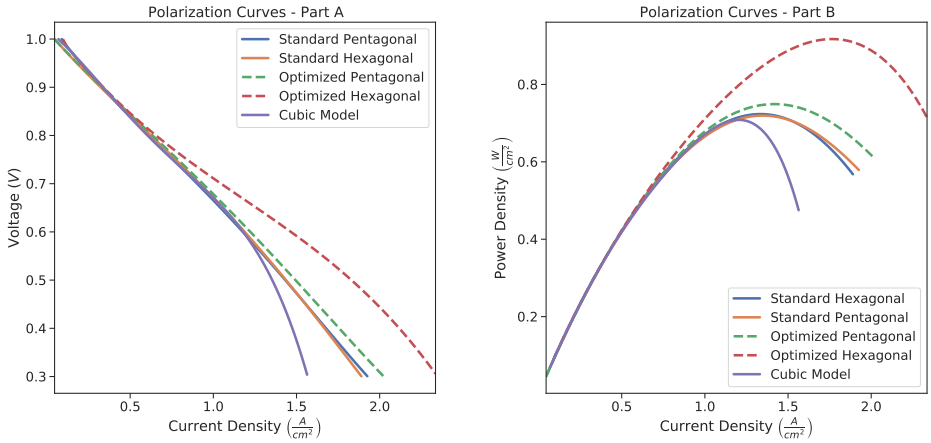

(a) Part 1 (b) Part 2

Figure 7: Polarization Curves of the Models

First, standard models perform better than base models. The Pentagonal and Hexagonal models have an average current density of 19.096% and

15.179% higher than the base model. Second, the current densities generated by the optimized models are even higher than the standard models, which are shown in Figure 8. The optimized pentagonal and hexagonal models have an average current density of 21.819% and 39.931% higher than the base model.

Two main reasons for these enhancements are optimal parameters and the new cell design. The performance of the presented models at near-open voltage is relatively similar to the cubic model. However, at low voltages, their performance has significantly enhanced.

Table 5: Differences of output current densities between models

	Max Difference	Avg. Difference
Pentagonal: Optimized vs. Standard	4.32301%	2.722995%
Pentagonal: Standard vs. Cubic	36.1996959%	19.0965193%
Pentagonal: Optimized vs. Cubic	45.9686959%	21.8195143%
Hexagonal: Optimized vs. Standard	44.5397%	24.7520657%
Hexagonal: Standard vs. Cubic	32.6451959%	15.1794143%
Hexagonal: Optimized vs. Cubic	77.1848959%	39.93148%

3.3. Effects of Relative Humidity

Figure 9 displays the effect of Relative Humidity (RH) on the performance of the standard presented fuel cell models. Humidity is among the main factors influencing fuel cell performance. Decreasing RH causes a reduction in the membrane's proton transfer conductivity in both cases. Overall, decreasing RH may decrease electrode kinetics, including electrode reaction and mass diffusion rates and membrane proton conductivity, leading to a severe decrease

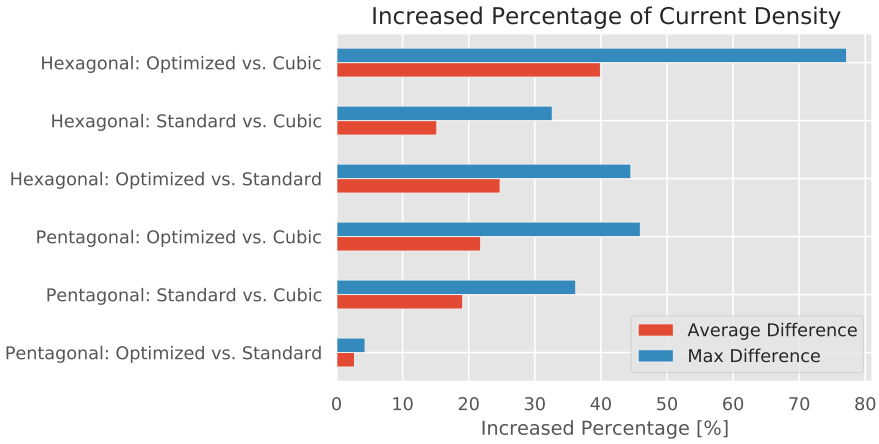

Figure 8: Increased percentage of current density of the presented models

in cell efficiency. According to this result, 100% humidity is reported to achieve adequate performance for both models.

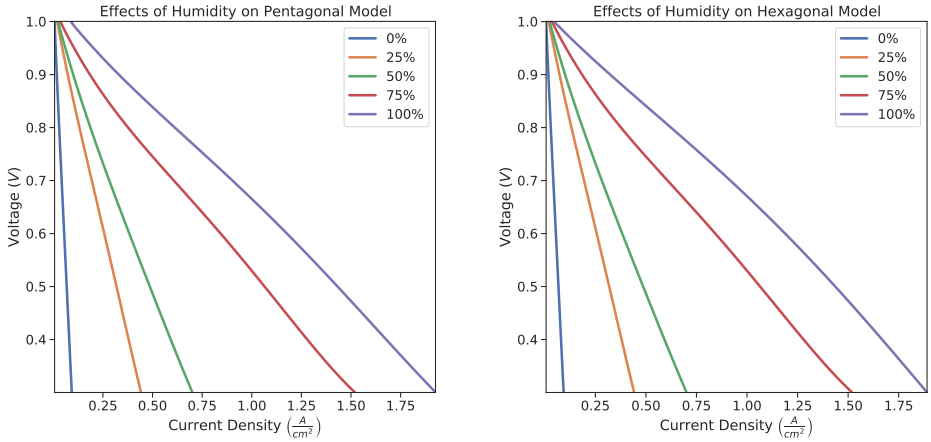

(a) Pentagonal Model

(b) Hexagonal model

Figure 9: Effects of humidity changes on models

3.4. Liquid Water Content

The amount of liquid water in the MEA influences the proton conductivity and the activation overpotential. If MEA is not sufficiently hydrated, proton conduction drops, and cell resistance increases. On the other hand, surplus water can cause problems in fuel cells, including water flooding. Figure 10 shows the volumetric average of water content in the layers of the standard presented models. Since This content is minimal in the anode part, we only displayed the cathode sections' water content. The water content at humidities below 100% is minimal in the fuel cell layers. This reduction in water content may cause the membrane to dry out and ultimately reduce the efficiency of the fuel cell.

The amounts of water in both models are close to each other. At 0.355v and 0.375v, the cathode layers of both the hexagonal and pentagonal models contain the highest water content.

4. Conclusion

This paper presented two new designs for PEM fuel cells with pentagonal and hexagonal shapes. After observing the increase in performance of these models compared to the cubic model in generating current density and electrical power, we optimized them. We modeled the data using neural networks and regression techniques. We used Response Surface Method *(RSM)* to derive the mathematical function corresponding to the problem objectives: production and consumption power. Then, using a multi-objective genetic optimization algorithm (*NSGA-II*), we simultaneously optimized these goals for the problem inputs, namely operating temperature and operating

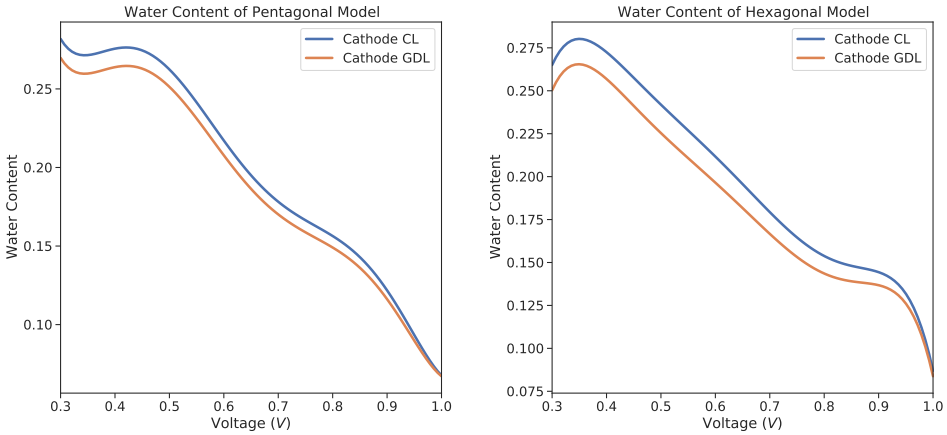

(a) Pentagonal Model (b) Hexagonal model

Figure 10: Effects of humidity changes on models

pressure. Having the optimal values for these models, we compared the optimized results with the results of standard models. Furthermore, We compared the effects of changes in the inlet relative humidity of the cell inlets in the models and examined the amount of liquid water.

The optimal designs outperform the base model (Cubic Model) and are more effective than the standard models. The average increase in output current density of the optimal models compared to the base model (Cubic) is 21.819% and 39.931% in the pentagonal and hexagonal models. Compared to optimized and standard cases, the mentioned percentage is 2.722% and 24.752% in the pentagonal and hexagonal models. We investigated the effect of relative humidity (RH) on the channel inputs of standard models. 100% humidity is the optimal setting for achieving the highest possible current density in the models. Reducing the relative humidity of the inlet causes the

MEA to dehydrate, reducing the current density and ultimately reducing the cell efficiency. We measured the average volumetric volume of liquid water content in the cathode section layers. For standard pentagonal and hexagonal models, the corresponding voltages for the highest liquid water contents are 0.379v and 0.355v.

References

[1] M. F. Akorede, H. Hizam, E. Pouresmaeil, Distributed energy resources and benefits to the environment, Renewable and sustainable energy reviews 14 (2010) 724–734.

[2] P. A. Owusu, S. Asumadu-Sarkodie, A review of renewable energy sources, sustainability issues and climate change mitigation, Cogent Engineering 3 (2016) 1167990.

[3] Y. Wang, K. S. Chen, J. Mishler, S. C. Cho, X. C. Adroher, A review of polymer electrolyte membrane fuel cells: Technology, applications, and needs on fundamental research, Applied energy 88 (2011) 981–1007.

[4] F. Barbir, Pem fuel cells, in: Fuel Cell Technology, Springer, 2006, pp. 27–51.

[5] S. J. Peighambardoust, S. Rowshanzamir, M. Amjadi, Review of the proton exchange membranes for fuel cell applications, International journal of hydrogen energy 35 (2010) 9349–9384.

[6] J. Hamelin, K. Agbossou, A. Laperriere, F. Laurencelle, T. Bose, Dy-

namic behavior of a pem fuel cell stack for stationary applications, International Journal of Hydrogen Energy 26 (2001) 625–629.

[7] D. Banham, S. Ye, Current status and future development of catalyst materials and catalyst layers for proton exchange membrane fuel cells: an industrial perspective, ACS Energy Letters 2 (2017) 629–638.

[8] J. P. Owejan, J. J. Gagliardo, J. M. Sergi, S. G. Kandlikar, T. A. Trabold, Water management studies in pem fuel cells, part i: Fuel cell design and in situ water distributions, International Journal of Hydrogen Energy 34 (2009) 3436–3444.

[9] P. Berg, K. Promislow, J. S. Pierre, J. Stumper, B. Wetton, Water management in pem fuel cells, Journal of the Electrochemical Society 151 (2004) A341.

[10] A. Öztürk, A. B. Yurtcan, Investigation of synergetic effect of pdms polymer hydrophobicity and polystyrene-silica particles roughness in the content of microporous layer on water management in pem fuel cell, Applied Surface Science 511 (2020) 145415.

[11] M. Rahimi-Esbo, A. Ramiar, A. Ranjbar, E. Alizadeh, Design, manufacturing, assembling and testing of a transparent pem fuel cell for investigation of water management and contact resistance at dead-end mode, International Journal of Hydrogen Energy 42 (2017) 11673–11688.

[12] Z. Liu, J. Chen, H. Liu, C. Yan, Y. Hou, Q. He, J. Zhang, D. Hissel, Anode purge management for hydrogen utilization and stack durability improvement of pem fuel cell systems, Applied Energy 275 (2020) 115110.

[13] J. Xu, C. Zhang, R. Fan, H. Bao, Y. Wang, S. Huang, C. S. Chin, C. Li, Modelling and control of vehicle integrated thermal management system of pem fuel cell vehicle, Energy 199 (2020) 117495.

[14] B. Zhang, F. Lin, C. Zhang, R. Liao, Y.-X. Wang, Design and implementation of model predictive control for an open-cathode fuel cell thermal management system, Renewable Energy 154 (2020) 1014–1024.

[15] W.-W. Yuan, K. Ou, Y.-B. Kim, Thermal management for an air coolant system of a proton exchange membrane fuel cell using heat distribution optimization, Applied Thermal Engineering 167 (2020) 114715.

[16] E. Carcadea, M. Varlam, M. Ismail, D. B. Ingham, A. Marinoiu, M. Raceanu, C. Jianu, L. Patularu, D. Ion-Ebrasu, Pem fuel cell performance improvement through numerical optimization of the parameters of the porous layers, International Journal of Hydrogen Energy 45 (2020) 7968–7980.

[17] H. Lan, L. Yang, F. Zheng, C. Zong, S. Wu, X. Song, Analysis and optimization of high temperature proton exchange membrane (ht-pem) fuel cell based on surrogate model, International Journal of Hydrogen Energy 45 (2020) 12501–12513.

[18] G. Cai, Y. Liang, Z. Liu, W. Liu, Design and optimization of bio-inspired wave-like channel for a pem fuel cell applying genetic algorithm, Energy 192 (2020) 116670.

[19] B. Wang, B. Xie, J. Xuan, K. Jiao, Ai-based optimization of pem fuel

cell catalyst layers for maximum power density via data-driven surrogate modeling, Energy Conversion and Management 205 (2020) 112460.

[20] M. Pan, C. Li, J. Liao, H. Lei, C. Pan, X. Meng, H. Huang, Design and modeling of pem fuel cell based on different flow fields, Energy 207 (2020) 118331.

[21] F. Mojica, M. A. Rahman, J. Mora, J. Ocon, P.-Y. Chuang, Experimental study of three channel designs with model comparison in a pem fuel cell, Fuel Cells 20 (2020) 547–557.

[22] M. A. A. Abdollahi, S. Jafarmadar, A. Jabbary, S. R. Amini Niaki, Effect of cathode-side gas flow channels section geometry on the removal process of liquid slug in a proton exchange membrane fuel cell, Proceedings of the Institution of Mechanical Engineers, Part E: Journal of Process Mechanical Engineering (2022) 09544089221086391.

[23] Y. Shao, L. Xu, X. Zhao, J. Li, Z. Hu, C. Fang, J. Hu, D. Guo, M. Ouyang, Comparison of self-humidification effect on polymer electrolyte membrane fuel cell with anodic and cathodic exhaust gas recirculation, International Journal of Hydrogen Energy 45 (2020) 3108–3122.

[24] X. Zhao, L. Xu, C. Fang, H. Jiang, J. Li, M. Ouyang, Study on voltage clamping and self-humidification effects of pem fuel cell system with dual recirculation based on orthogonal test method, International Journal of Hydrogen Energy 43 (2018) 16268–16278.

[25] T. Wilberforce, O. Ijaodola, F. Khatib, E. Ogungbemi, Z. El Hassan, J. Thompson, A. Olabi, Effect of humidification of reactive gases on the

performance of a proton exchange membrane fuel cell, Science of The Total Environment 688 (2019) 1016–1035.

[26] Z. Liu, J. Chen, S. Chen, L. Huang, Z. Shao, Modeling and control of cathode air humidity for pem fuel cell systems, IFAC-PapersOnLine 50 (2017) 4751–4756.

[27] K. Subin, P. Jithesh, Experimental study on self-humidified operation in pem fuel cells, Sustainable Energy Technologies and Assessments 27 (2018) 17–22.

[28] Y. Cao, H. Ayed, S. Jafarmadar, M. A. A. Abdollahi, A. Farag, M. Waehayee, M. Hashemian, Pem fuel cell cathode-side flow field design optimization based on multi-criteria analysis of liquid-slug dynamics, Journal of Industrial and Engineering Chemistry 98 (2021) 397–412.

[29] J. Wang, Theory and practice of flow field designs for fuel cell scaling-up: a critical review, Applied Energy 157 (2015) 640–663.

[30] T. Berning, D. Lu, N. Djilali, Three-dimensional computational analysis of transport phenomena in a pem fuel cell, Journal of power sources 106 (2002) 284–294.

[31] A. Manso, F. Marzo, J. Barranco, X. Garikano, M. G. Mujika, Influence of geometric parameters of the flow fields on the performance of a pem fuel cell. a review, International journal of hydrogen energy 37 (2012) 15256–15287.

[32] X. Li, I. Sabir, Review of bipolar plates in pem fuel cells: Flow-field designs, International journal of hydrogen energy 30 (2005) 359–371.

[33] T. Wilberforce, Z. El Hassan, E. Ogungbemi, O. Ijaodola, F. Khatib, A. Durrant, J. Thompson, A. Baroutaji, A. Olabi, A comprehensive study of the effect of bipolar plate (bp) geometry design on the performance of proton exchange membrane (pem) fuel cells, Renewable and Sustainable Energy Reviews 111 (2019) 236–260.

[34] P. Dong, G. Xie, M. Ni, Improved energy performance of a pem fuel cell by introducing discontinuous s-shaped and crescent ribs into flowing channels, Energy 222 (2021) 119920.

[35] M. Asadzade, A. Shamloo, Design and simulation of a novel bipolar plate based on lung-shaped bio-inspired flow pattern for pem fuel cell, International Journal of Energy Research 41 (2017) 1730–1739.

[36] M. Seyhan, Y. E. Akansu, M. Murat, Y. Korkmaz, S. O. Akansu, Performance prediction of pem fuel cell with wavy serpentine flow channel by using artificial neural network, International Journal of Hydrogen Energy 42 (2017) 25619–25629.

[37] E. Afshari, M. Ziaei-Rad, M. M. Dehkordi, Numerical investigation on a novel zigzag-shaped flow channel design for cooling plates of pem fuel cells, Journal of the Energy Institute 90 (2017) 752–763.

[38] A. Jabbary, S. Rostami Arnesa, H. Samanipour, N. Ahmadi, Numerical investigation of 3d rhombus designed pemfc on the cell performance, International Journal of Green Energy 18 (2021) 425–442.

[39] H. Samanipour, N. Ahmadi, A. Jabbary, Effects of applying brand-new designs on the performance of pem fuel cell and water flooding

phenomena, Iranian Journal of Chemistry and Chemical Engineering (IJCCE) (2020).

[40] C. Wang, C. Yan, J. Wang, C. Tian, S. Yu, Parametric optimization of steam cycle in pwr nuclear power plant using improved genetic-simplex algorithm, Applied Thermal Engineering 125 (2017) 830–845.

[41] T. Fletcher, R. Thring, M. Watkinson, An energy management strategy to concurrently optimise fuel consumption & pem fuel cell lifetime in a hybrid vehicle, international journal of hydrogen energy 41 (2016) 21503–21515.

[42] U. Sarma, S. Ganguly, Design optimisation for component sizing using multi-objective particle swarm optimisation and control of pem fuel cell-battery hybrid energy system for locomotive application, IET Electrical Systems in Transportation 10 (2020) 52–61.

[43] A. A. El-Fergany, H. M. Hasanien, A. M. Agwa, Semi-empirical pem fuel cells model using whale optimization algorithm, Energy Conversion and Management 201 (2019) 112197.

[44] R. Vatankhah Barenji, M. Ghadiri Nejad, I. Asghari, Optimally sized design of a wind/photovoltaic/fuel cell off-grid hybrid energy system by modified-gray wolf optimization algorithm, Energy & Environment 29 (2018) 1053–1070.

[45] G. Lei, H. Song, D. Rodriguez, Power generation cost minimization of the grid-connected hybrid renewable energy system through optimal

sizing using the modified seagull optimization technique, Energy Reports 6 (2020) 3365–3376.

[46] S. Bai, L. Wang, X. Wang, Optimization of ejector geometric parameters with hybrid artificial fish swarm algorithm for pem fuel cell, in: 2017 Chinese Automation Congress (CAC), IEEE, 2017, pp. 3319–3322.

[47] Y. Cao, Y. Li, G. Zhang, K. Jermsittiparsert, N. Razmjooy, Experimental modeling of pem fuel cells using a new improved seagull optimization algorithm, Energy Reports 5 (2019) 1616–1625.

[48] D. Miao, W. Chen, W. Zhao, T. Demsas, Parameter estimation of pem fuel cells employing the hybrid grey wolf optimization method, Energy 193 (2020) 116616.

[49] D. Song, Q. Wang, Z. Liu, T. Navessin, M. Eikerling, S. Holdcroft, Numerical optimization study of the catalyst layer of pem fuel cell cathode, Journal of Power Sources 126 (2004) 104–111.

[50] S. Sivanandam, S. Deepa, Genetic algorithms, in: Introduction to genetic algorithms, Springer, 2008, pp. 15–37.

[51] F. Dehghanian, S. Mansour, Designing sustainable recovery network of end-of-life products using genetic algorithm, Resources, Conservation and Recycling 53 (2009) 559–570.

[52] Y. K. Dwivedi, L. Hughes, E. Ismagilova, G. Aarts, C. Coombs, T. Crick, Y. Duan, R. Dwivedi, J. Edwards, A. Eirug, et al., Artificial intelligence (ai): Multidisciplinary perspectives on emerging challenges, opportunities,

and agenda for research, practice and policy, International Journal of Information Management (2019) 101994.

[53] S.-L. Wamba-Taguimdje, S. F. Wamba, J. R. K. Kamdjoug, C. E. T. Wanko, Influence of artificial intelligence (ai) on firm performance: the business value of ai-based transformation projects, Business Process Management Journal (2020).

[54] F. Tao, Q. Qi, A. Liu, A. Kusiak, Data-driven smart manufacturing, Journal of Manufacturing Systems 48 (2018) 157–169.

[55] C.-Y. Wang, Fundamental models for fuel cell engineering, Chemical reviews 104 (2004) 4727–4766.

[56] S. A. Atyabi, E. Afshari, Three-dimensional multiphase model of proton exchange membrane fuel cell with honeycomb flow field at the cathode side, Journal of cleaner production 214 (2019) 738–748.

[57] X. Zhou, T. Zhao, Y. Zeng, L. An, L. Wei, A highly permeable and enhanced surface area carbon-cloth electrode for vanadium redox flow batteries, Journal of Power Sources 329 (2016) 247–254.

[58] S. Toghyani, E. Afshari, E. Baniasadi, S. Atyabi, Thermal and electrochemical analysis of different flow field patterns in a pem electrolyzer, Electrochimica Acta 267 (2018) 234–245.

[59] M. K. Das, P. P. Mukherjee, K. Muralidhar, Equations governing flow and transport in porous media, in: Modeling Transport Phenomena in Porous Media with Applications, Springer, 2018, pp. 15–63.

[60] B. R. Sivertsen, N. Djilali, Cfd-based modelling of proton exchange membrane fuel cells, Journal of Power Sources 141 (2005) 65–78.

[61] P. K. Das, X. Li, Z.-S. Liu, A three-dimensional agglomerate model for the cathode catalyst layer of pem fuel cells, Journal of Power Sources 179 (2008) 186–199.

[62] P. K. Das, X. Li, Z.-S. Liu, Analysis of liquid water transport in cathode catalyst layer of pem fuel cells, International Journal of Hydrogen Energy 35 (2010) 2403–2416.

[63] T. E. Springer, T. Zawodzinski, S. Gottesfeld, Polymer electrolyte fuel cell model, Journal of the electrochemical society 138 (1991) 2334.

[64] F. Hashemi, S. Rowshanzamir, M. Rezakazemi, Cfd simulation of pem fuel cell performance: effect of straight and serpentine flow fields, Mathematical and Computer Modelling 55 (2012) 1540–1557.

[65] W. A. Mulder, A new multigrid approach to convection problems, Journal of Computational Physics 83 (1989) 303–323.

[66] M. Abadi, A. Agarwal, P. Barham, E. Brevdo, Z. Chen, C. Citro, G. S. Corrado, A. Davis, J. Dean, M. Devin, et al., Tensorflow: Large-scale machine learning on heterogeneous distributed systems, arXiv preprint arXiv:1603.04467 (2016).

[67] D. B. Fogel, An introduction to simulated evolutionary optimization, IEEE transactions on neural networks 5 (1994) 3–14.